CONSERVATION LAWS FOR ONE- AND MULTI-COMPONENT GASES
WITH AND WITHOUT SOURCE TERMS

Simulation of a shock tube experiment with non-equilibrium chemistry

Ralf Deiterding
Institute of Mathematics, Technical University Cottbus, Germany
e-mail: deiterding@math.tu-cottbus.de

Technical Report NMWR-00-3
October 20, 2000

1 Introduction

Flows of mixtures of several chemically reacting gaseous species can be modeled by generalized Euler equations. The model is valid, if aspects of wave propagation, like shocks or combustions waves, are of primary interest and diffusive effects can be neglected. The most simple examples for this type of reactive flows are shock tube experiments, if fuel and oxidizer are already premixed.

In this report, we simulate the ignition process of a hydrogen-oxygen-argon mixture in a shock tube closed at one end due to reflection of a shock wave. A strong detonation wave arises at the boundary and runs through the tube with supersonic speed. It overtakes the reflected shock leaving the former shock now traveling as a contact discontinuity behind.

This particular one-dimensional example has been studied intensively in the past [9] and especially a well validated reaction mechanism for numerical simulations is available today [8, 9]. It utilizes 9 different chemical species and 48 non-equilibrium elementary reactions. The complexity of this mechanism is moderate and qualitative correct numerical results for the shock tube ignition experiment can be obtained with mean computational effort. Quantitative correct computations require a higher expense and can serve as an accurate test case for new numerical methods (e.g. [2]).

2 Governing equations

The one-dimensional Euler equations with chemical reactive source terms take the following form:

$$\begin{array}{lcll} \partial_t \rho_i & + & \partial_x(\rho_i u) & = W_i\,\dot{\omega}_i \qquad i = 1,\ldots,K \\ \partial_t(\rho u) & + & \partial_x(\rho u^2 + p) & = 0 \\ \partial_t(\rho E) & + & \partial_x\left[u(\rho E + p)\right] & = 0 \end{array} \tag{1}$$

For each gaseous species a continuity equation is utilized. Herein ρ_i denotes the partial density, while the mass production rate due to chemical reaction is written as $W_i\ \dot{\omega}_i$ (see appendix A.1 for the actual reaction mechanism). E is the total energy per unit mass and u is the velocity in x-direction. The hydrodynamic pressure p is evaluated by Dalton's law for mixtures of ideal gases. A more detailed explanation of Euler equations with reactive source terms with non-equilibrium chemistry and the necessary thermodynamic relations is given in [1].

3 Geometry

The shock tube has a length of 12 cm. Its geometry is simplified to a closed one-dimensional interval.

4 Initial conditions

The entire shock tube is filled with a stoichiometric H_2:O_2:Ar-mixture of molar ratios 2:1:7. Then, an incident shock wave is created that travels from right to left through the tube. When the incident shock wave hits the left boundary, it is reflected backwards. The reflected shock leaves a mixture with zero velocity but with an increased temperature behind. This temperature exceeds the ignition limit and a detonation wave forms.

To simplify considerations, we start the simulation exactly at the point, when the incident shock hits the left boundary. Consequently, the entire computational domain is initialized with the constant vector of state behind the incident shock (see tab. 1). This shock is immediately reflected and a new shock wave travels to the right with a shock speed of 411 m s^{-1}.

	Incident shock	Reflected shock
ρ [kg m^{-2}]	0.223128	0.4889
u [m s^{-1}]	-478.5	0.0
p [Pa]	36679.65	131820
T [°K]	624	1036
v_{cj} [m s^{-1}]	1631	1624
$X_{H_2} : X_{O_2} : X_{Ar}$	0.200000 : 0.100000 : 0.700000	
$Y_{H_2} : Y_{O_2} : Y_{Ar}$	0.012773 : 0.101369 : 0.885858	
W [kg mol^{-1}]	$3.156667 \cdot 10^{-2}$	

Table 1: Initial data (incident shock) and values behind reflected shock. Chapman-Jouguet velocities have been calculated using the Gaseq-program [7].

5 Boundary conditions

Solid wall boundary conditions at $x = 0$ cm. Constant inflow at $x = 12$ cm.

6 Simulation

The chemical induction time in the mixture behind the reflected shock is approximately 108μs (see fig. 2). After this induction period a detonation wave develops near the left boundary. Its propagation velocity converges to the Chapman-Jouguet velocity 1624 m s^{-1}. Before the detonation reaches the Chapman-Jouguet limit, it catches up with the reflected shock and the state in the unburned gas in front of the detonation suddenly changes. The Chapman-Jouguet velocity for the new unburned state is 1631 m s^{-1} and the detonation now decelerates towards this limit due to the incident flow velocity of -478.5 m s^{-1}. After merging with the detonation front the reflected shock wave travels as a contact discontinuity with decreased

speed. Fig. 1 shows the positions of the involved wave fronts during simulation and the propagation velocity of the detonation wave.

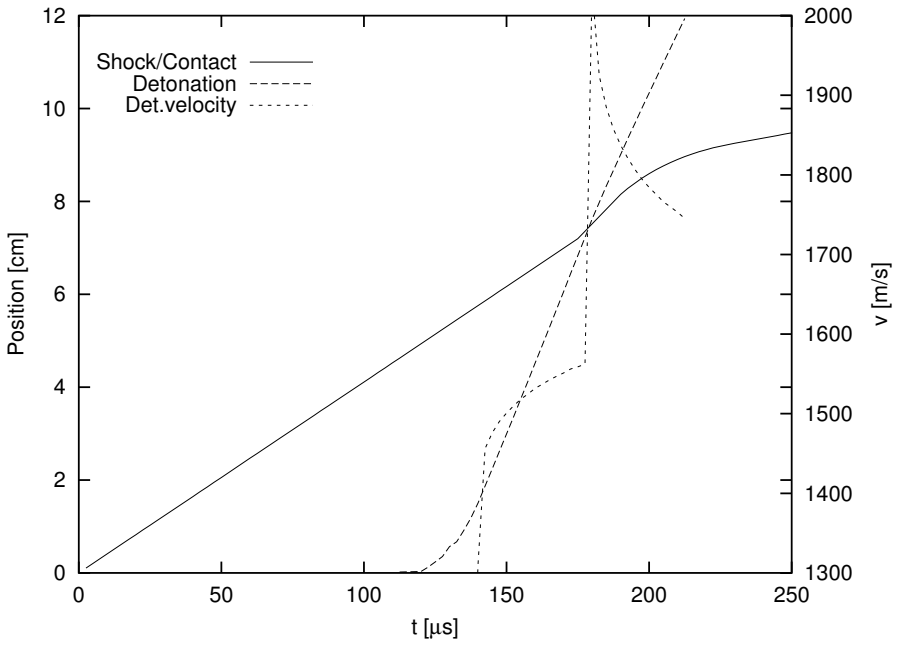

Figure 1: Positions of wave fronts and approximated detonation velocity as a function of time for a highly resolved simulation with 4800 cells.

7 Required output

Five calculations on equally spaced grids with mesh widths h=0.04 cm, 0.02 cm, 0.01 cm, 0.005 cm and 0.0025 cm should be carried out. All computations end at 210 μs, before the detonation wave hits the right boundary. For the comparative data variable time steps yielding a CFL-No. around 0.8 have been used.

- A detailed description of the numerical algorithm is required.
  1. Hydrodynamic transport scheme.
  2. Incorporation of source terms (split or unsplit).
  3. Treatment of stiff source terms.
- For each computation a plot like fig. 1 showing the positions of the wave fronts and the approximated detonation velocity as a function of time should be generated.
- The point when detonation and reflected shock wave merge should be measured exactly and a table like tab. 2 should be created. The propagation velocity of the reflected shock will be calculated correctly by any conservative scheme, but the approximated detonation velocity will depend strongly on the numerical algorithm and especially on the discretization. This point is therefore an appropriate simple quantity to measure the accuracy of the entire method. It should converge to a value of approximately 179μs.

8 Comparative data

We employ a fractional step method and alternate between solving the homogeneous hydrodynamic transport equations and a stiff system of ordinary differential equation for the chemical kinetics. For the pure hydrodynamic transport we solve

$$\begin{array}{lcll} \partial_t \rho_i & + & \partial_x(\rho_i u) & = 0 \qquad i = 1, \ldots, K \\ \partial_t(\rho u) & + & \partial_x(\rho u^2 + p) & = 0 \\ \partial_t(\rho E) & + & \partial_x\left[u(\rho E + p)\right] & = 0 \quad . \end{array} \tag{2}$$

The wave propagation method of R. J. LeVeque [6] in combination with an approximate Riemann solver of Roe type for mixtures of real gases is utilized (see [3] for necessary Roe averages). After each transport step, we integrate

$$\partial_t \rho_i = W_i \, \dot{\omega}_i(\rho_1, \ldots, \rho_K, T) \qquad i = 1, \ldots, K \tag{3}$$

to incorporate the reactive source terms. Within each grid cell (3) can be solved separately with a standard ODE method. ODE systems that arise in chemical kinetics are usually stiff and we employ a semi-implicit Rosenbrock-Wanner method by Kaps and Rentrop of fourth order with automatic stepsize adjustment [4]. Note that ρ, e, u are assumed to be constant during ODE integration and in each grid cell the chemical kinetics are computed like in the zero-dimensional constant volume adiabatic case (compare A.3).

Whenever the temperature T has to be calculated from the conserved variables the implicit equation

$$\sum_{i=1}^{K} \rho_i \, h_i(T) - \mathcal{R}T \sum_{i=1}^{K} \frac{\rho_i}{W_i} - \rho E + \rho \frac{u^2}{2} = 0 \tag{4}$$

is solved utilizing Newton's method [1]. The iteration is initialized with the temperature value of the preceding time step, which has to be therefore stored for any grid cell.

Tab. 2 gives results that have been obtained with the described algorithm on different grids. Fig. 3-6 show the reference data calculated on a grid with 2400 cells at different time steps.

Cells	$t_m[\mu s]$	CPU [h]
300	169.5	0.21
600	175.0	0.60
1200	177.0	1.7
2400	178.2	4.7
4800	178.7	13

Table 2: Calculated times at which detonation wave and reflected shock merge. Necessary CPU-time on Pentium-III-system with 450 MHz for whole computation.

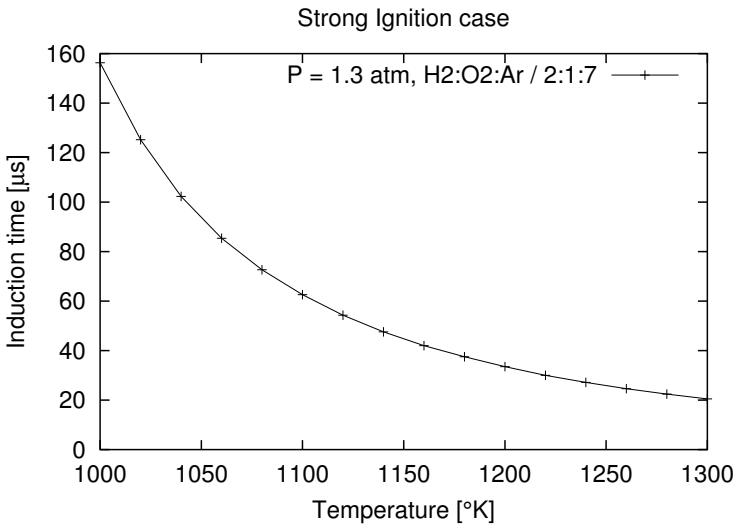

Figure 2: Chemical induction time as a function of temperature [9].

References

[1] R. Deiterding. Generalized euler equations with non-equilibirum chemistry. Technical Report NMWR-00-2, Brandenburgische Technische Universität Cottbus, Oct 2000. Available on the web at `http://www.math.tu-cottbus.de/~deiter/pub/nmwr_00_2.ps.gz`.

[2] R. P. Fedkiw, B. Merriman, and S. Osher. High accuracy numerical methods for thermally perfect gas flows with chemistry. *J. Comput. Phys.*, 132:175–190, 1997.

[3] B. Grossmann and P. Cinella. Flux-split algorithms for flows with non-equilibrium chemistry and vibrational relaxation. *J. Comput. Phys.*, 88:131–168, 1990.

[4] P. Kaps and P. Rentrop. *Numerische Mathematik*, 33:55–68, 1979.

[5] R. J. Kee, F. M. Rupley, and J. A. Miller. *Chemkin-II: A Fortran chemical kinetics package for the analysis of gas-phase chemical kinetics.* SAND89-8009, Sandia National Laboratories, Livermore, California, Sep 1989.

[6] R. J. LeVeque. Wave propagation algorithms for multidimensional hyperbolic systems. *J. Comput. Phys.*, 131(2):327–353, 1997.

[7] C. Morley. Gaseq: A chemical equilibrium program for Windows. Available on the web at `http://www.c.morley.ukgateway.net`.

[8] E. S. Oran and J. P. Boris. Theoretical and computational approach to modelling flame ignition. *Prog. Aeronautics Astronautics*, 76:154–171, 1981.

[9] E. S. Oran, T. R. Young, J. P. Boris, and A. Cohen. Weak and strong ignition. I. Numerical simulation of shock tube experiments. *J. Combustion and Flame*, 48:135–148, 1982.

A Chemical kinetics

A.1 Reaction mechanism

The hydrogen-oxygen-argon mechanism from [8, 9] is displayed in tab. 3.

A.2 Thermodynamic data

Necessary thermodynamic data are extracted from the Chemkin-II data base [5]. The employed thermodynamic fits are valid for a temperature range from $300°K$ to $5000°K$.

A.3 Validation of reaction mechanism

Before a reactive flow problem can be simulated successively the chemical kinetics alone have to be verified. This is usually done by carrying out separate zero-dimensional calculations for chemical induction times. We consider the constant volume adiabatic case for which (1) reduces to

$$\begin{aligned} \partial_t \rho_i &= W_i \, \dot{\omega}_i \qquad i = 1, \ldots, K \\ \partial_t e &= 0 \quad . \end{aligned} \tag{5}$$

Note that (5) is an implicit ODE system for the independent variables $\rho_1, \ldots, \rho_K$ and T. The solution of a given initial-value problem for (5) can heavily be simplified, if (5) is transformed into the following explicit system:

$$\begin{aligned} \partial_t \rho_i &= W_i \;\; \dot{\omega}_i(\rho_1, \ldots, \rho_K, T) \qquad\qquad i = 1, \ldots, K \\ \partial_t T &= \frac{\sum_{i=1}^{K} (W_i \, h_i(T) - \mathcal{R}T) \, \dot{\omega}_i(\rho_1, \ldots, \rho_K, T)}{\rho \, (\mathcal{R}/W - c_p(T))} \end{aligned}$$

with $c_p(T) = \sum_{i=1}^{K} Y_i \, c_{pi}(T)$.

Alternatively, equally good results are obtained in practice, if only the system

$$\partial_t \rho_i = W_i \, \dot{\omega}_i(\rho_1, \ldots, \rho_K, T) \qquad i = 1, \ldots, K$$

is used and T is derived from the implicit equation

$$\sum_{i=1}^{K} \rho_i \, h_i(T) - \mathcal{R}T \sum_{i=1}^{K} \frac{\rho_i}{W_i} - \rho e = 0 \quad .$$

Following [9] we now compute induction times for a H_2:O_2:Ar-mixture of molar ratios 2:1:7 in a perfectly stirred constant volume adiabatic vessel. The initial pressure is always 131820 Pa = 1.3 atm, while the initial temperature (and therefore the initial density) varies. The induction time is defined as the point at which the initial temperature increases by 20°K. Fig. 2 displays the results of this computation.

A.4 Units

In our computational code we utilize the Chemkin-II library to evaluate chemical production rates. To avoid permanent conversion the code internally employs the fixed unit system determined by Chemkin-II [5]. In this report, we use SI-units for initial conditions and reference data. Tab. 5 gives the necessary factors to convert initial data and output into the Chemkin-II unit system.

								A [cm, mol, s]	β	E_{act} [cal mol^{-1}]
1.	H	+ OH		$\longrightarrow$	O	+ H_2		$0.843E+10$	1.00	6955
2.	O	+ H_2		$\longrightarrow$	H	+ OH		$0.181E+11$	1.00	8903
3.	H	+ HO_2		$\longrightarrow$	H_2	+ O_2		$0.253E+14$	0.00	696
4.	H_2	+ O_2		$\longrightarrow$	H	+ HO_2		$0.548E+14$	0.00	57828
5.	H	+ HO_2		$\longrightarrow$	OH	+ OH		$0.253E+15$	0.00	1888
6.	OH	+ OH		$\longrightarrow$	H	+ HO_2		$0.120E+14$	0.00	40142
7.	H	+ HO_2		$\longrightarrow$	O	+ H_2O		$0.500E+14$	0.00	994
8.	O	+ H_2O		$\longrightarrow$	H	+ HO_2		$0.105E+13$	0.45	56437
9.	H	+ H_2O_2		$\longrightarrow$	HO_2	+ H_2		$0.169E+13$	0.00	3776
10.	HO_2	+ H_2		$\longrightarrow$	H	+ H_2O_2		$0.723E+12$	0.00	18680
11.	H	+ H_2O_2		$\longrightarrow$	OH	+ H_2O		$0.318E+15$	0.00	8943
12.	OH	+ H_2O		$\longrightarrow$	H	+ H_2O_2		$0.240E+15$	0.00	80483
13.	OH	+ H_2		$\longrightarrow$	H	+ H_2O		$0.110E+10$	1.30	3657
14.	H	+ H_2O		$\longrightarrow$	OH	+ H_2		$0.108E+11$	1.20	19097
15.	OH	+ OH		$\longrightarrow$	H_2	+ O_2		$0.656E+11$	0.26	29212
16.	H_2	+ O_2		$\longrightarrow$	OH	+ OH		$0.169E+14$	0.00	48091
17.	OH	+ OH		$\longrightarrow$	O	+ H_2O		$0.602E+08$	1.30	0
18.	O	+ H_2O		$\longrightarrow$	OH	+ OH		$0.193E+10$	1.16	17428
19.	OH	+ HO_2		$\longrightarrow$	H_2O	+ O_2		$0.500E+14$	0.00	1000
20.	H_2O	+ O_2		$\longrightarrow$	OH	+ HO_2		$0.143E+15$	0.17	73329
21.	OH	+ H_2O_2		$\longrightarrow$	HO_2	+ H_2O		$0.102E+14$	0.00	1808
22.	HO_2	+ H_2O		$\longrightarrow$	OH	+ H_2O_2		$0.283E+14$	0.00	32789
23.	HO_2	+ H_2		$\longrightarrow$	OH	+ H_2O		$0.723E+12$	0.00	18700
24.	OH	+ H_2O		$\longrightarrow$	HO_2	+ H_2		$0.801E+10$	0.43	71938
25.	HO_2	+ HO_2		$\longrightarrow$	H_2O_2	+ O_2		$0.181E+14$	0.00	994
26.	H_2O_2	+ O_2		$\longrightarrow$	HO_2	+ HO_2		$0.945E+15$	−0.38	43719
27.	O	+ OH		$\longrightarrow$	H	+ O_2		$0.164E+13$	0.28	−161
28.	H	+ O_2		$\longrightarrow$	O	+ OH		$0.223E+15$	0.00	16792
29.	O	+ HO_2		$\longrightarrow$	OH	+ O_2		$0.501E+14$	0.00	1000
30.	OH	+ O_2		$\longrightarrow$	O	+ HO_2		$0.132E+14$	0.18	56040
31.	O	+ H_2O_2		$\longrightarrow$	H_2O	+ O_2		$0.843E+12$	0.00	4213
32.	H_2O	+ O_2		$\longrightarrow$	O	+ H_2O_2		$0.343E+11$	0.52	89028
33.	O	+ H_2O_2		$\longrightarrow$	OH	+ HO_2		$0.843E+12$	0.00	4233
34.	OH	+ HO_2		$\longrightarrow$	O	+ H_2O_2		$0.125E+10$	0.64	16355
35.	H_2	+ M		$\longrightarrow$	H	+ H	+ M	$0.223E+15$	0.00	95983
36.	H_2O	+ M		$\longrightarrow$	H	+ OH	+ M	$0.349E+16$	0.00	105124
37.	HO_2	+ M		$\longrightarrow$	H	+ O_2	+ M	$0.211E+16$	0.00	45706
38.	H_2O_2	+ M		$\longrightarrow$	OH	+ OH	+ M	$0.120E+18$	0.00	45508
39.	OH	+ M		$\longrightarrow$	O	+ H	+ M	$0.140E+15$	0.21	101349
40.	HO_2	+ M		$\longrightarrow$	O	+ OH	+ M	$0.662E+20$	−0.43	63989
41.	O_2	+ M		$\longrightarrow$	O	+ O	+ M	$0.181E+19$	−1.00	118041
42.	H	+ H	+ M	$\longrightarrow$	H_2	+ M		$0.653E+18$	−1.00	0
43.	H	+ OH	+ M	$\longrightarrow$	H_2O	+ M		$0.225E+23$	−2.00	0
44.	H	+ O_2	+ M	$\longrightarrow$	HO_2	+ M		$0.150E+16$	0.00	−994
45.	OH	+ OH	+ M	$\longrightarrow$	H_2O_2	+ M		$0.907E+15$	0.00	−5067
46.	O	+ H	+ M	$\longrightarrow$	OH	+ M		$0.300E+20$	−1.00	0
47.	O	+ OH	+ M	$\longrightarrow$	HO_2	+ M		$0.102E+18$	0.00	0
48.	O	+ O	+ M	$\longrightarrow$	O_2	+ M		$0.189E+14$	0.00	−1789

Table 3: Hydrogen-oxygen-argon mechanism from [8, 9] in units for Chemkin-II.

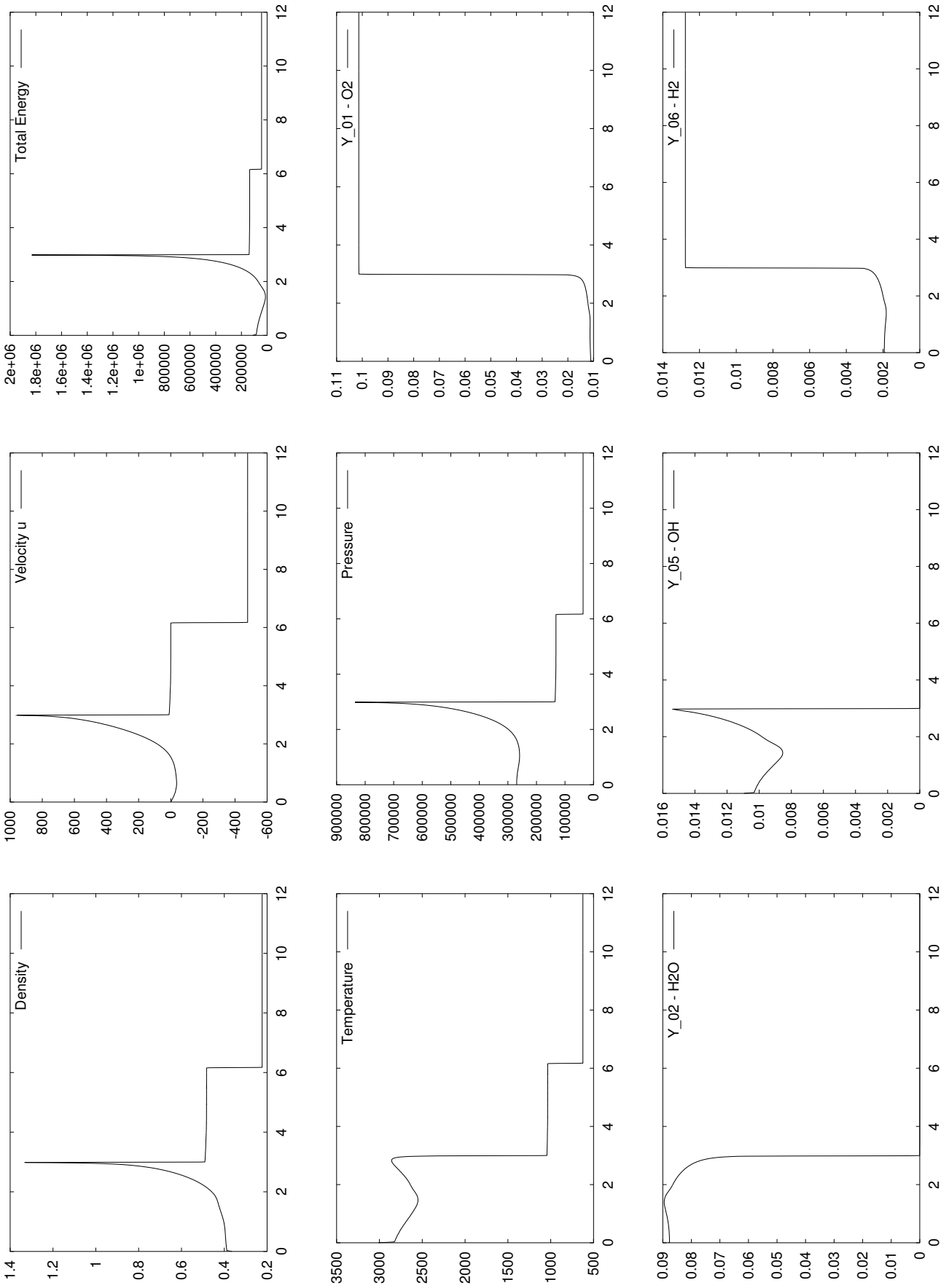

Figure 3: Reference data at t = 150 μs.

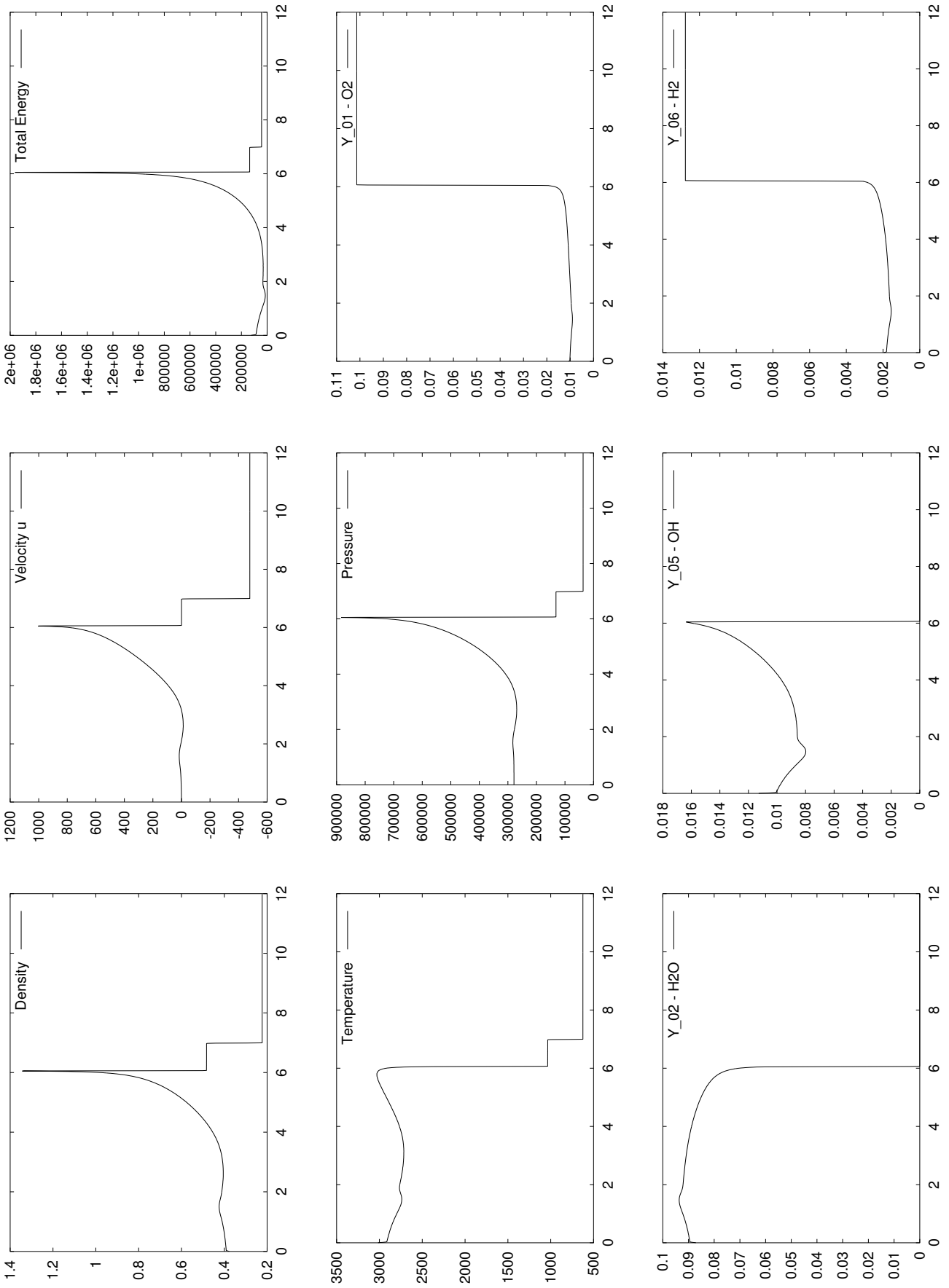

Figure 4: Reference data at t = 170 μs.

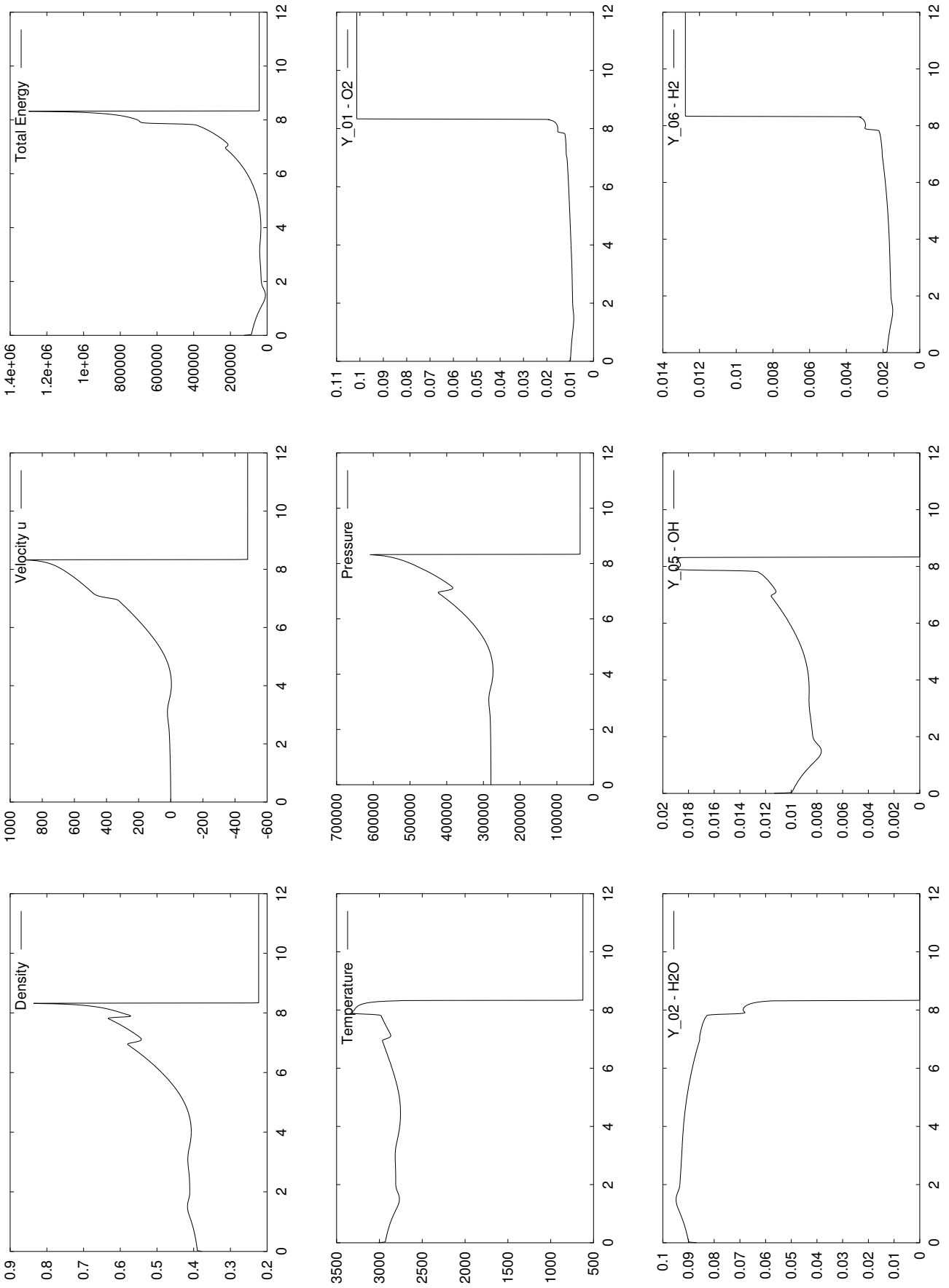

Figure 5: Reference data at t = 185 μs.

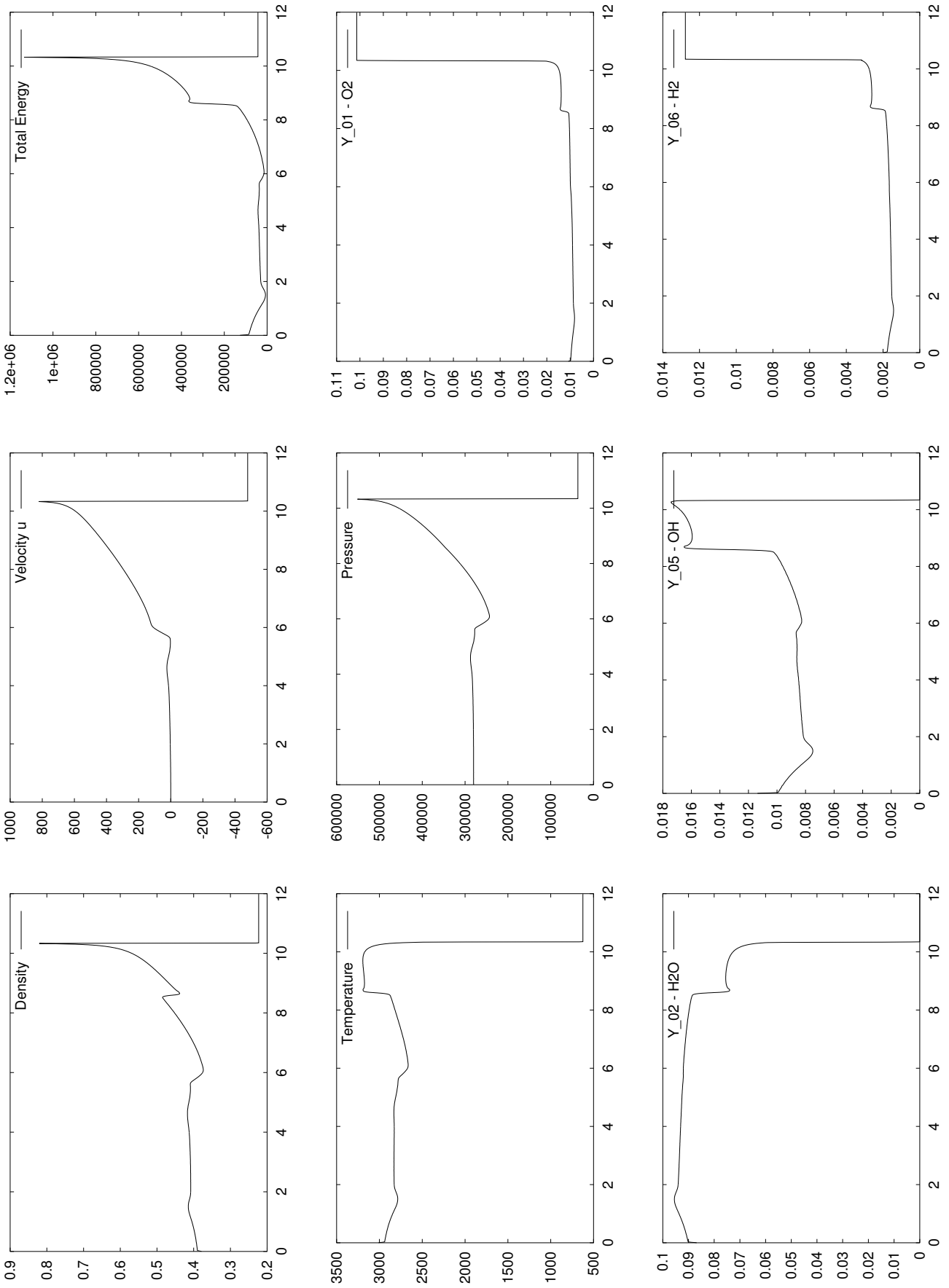

Figure 6: Reference data at t = 200 μs.

	W [g mol^{-1}]
H	1.0079700
O	15.999400
OH	17.007370
H_2	2.0159400
O_2	31.998800
H_2O	18.015340
HO_2	33.006770
H_2O_2	34.014740
Ar	39.948002

Table 4: Molecular weights of involved species [5].

	Chemkin-II (g, cm, mol, s)	SI (kg, m, mol, s)	Factor†
ρ	g cm^{-3}	kg m^{-3}	10^3
u	cm s^{-1}	m s^{-1}	10^{-2}
e, E	erg g^{-1}	J kg^{-1}	10^{-4}
h, h^f	erg g^{-1}	J kg^{-1}	10^{-4}
c_v, c_p	erg g^{-1} K^{-1}	J kg^{-1} K^{-1}	10^{-4}
ρE	erg cm^{-3}	J m^{-3}	10^{-1}
p	dyne cm^{-2}	N m^{-2}	10^{-1}
T	K	K	-
W	g mol^{-1}	kg mol^{-1}	10^{-3}
$\dot{\omega}$	mol cm^{-3} s^{-1}	mol m^{-3} s^{-1}	10^6
$\mathcal{R}$	$8.31441 \cdot 10^7$ erg mol^{-1} K^{-1}	8.31441 J mol^{-1} K^{-1}	10^{-7}
A^*	(cm^3 mol^{-1})$^{r-1}$ s^{-1}	(m^3 mol^{-1})$^{r-1}$ s^{-1}	$(10^{-6})^{r-1}$
β	-	-	-
E_{act}	cal mol^{-1}	J mol^{-1}	4.18392
$\mathcal{R}^{**}_{act}$	1.98723 cal mol^{-1} K^{-1}	8.31441 J mol^{-1} K^{-1}	4.18392

† Conversion factor from units used in Chemkin-II into SI-units. * r denotes the reaction order.
** used for activation energy within Chemkin-II.
1 erg = 1 g cm^2 s^{-2}, 1 J = 1 kg m^2 s^{-2}, 1 dyne = g cm s^{-2}, 1 Nm^{-2} = 1 Pa = kg m^{-1} s^{-2}
1 erg = 10^{-7} J = $2.3901 \cdot 10^{-8}$ cal, $1.01325 \cdot 10^5$ Pa = $1.01325 \cdot 10^6$ dyne cm^{-2} = 1 atm

Table 5: Conversion of Chemkin-II- into SI-units.